EUROPEAN ORGANIZATION FOR NUCLEAR RESEARCH (CERN)

CERN-EP-2020-075
2020/07/08

CMS-BPH-14-009

Investigation into the event-activity dependence of Υ(nS) relative production in proton-proton collisions at $\sqrt{s} = 7\,\text{TeV}$

The CMS Collaboration*

Abstract

The ratios of the production cross sections between the excited Υ(2S) and Υ(3S) mesons and the Υ(1S) ground state, detected via their decay into two muons, are studied as a function of the number of charged particles in the event. The data are from proton-proton collisions at $\sqrt{s} = 7\,\text{TeV}$, corresponding to an integrated luminosity of $4.8\,\text{fb}^{-1}$, collected with the CMS detector at the LHC. Evidence of a decrease in these ratios as a function of the particle multiplicity is observed, more pronounced at low transverse momentum $p_{\text{T}}^{\mu\mu}$. For Υ(nS) mesons with $p_{\text{T}}^{\mu\mu} > 7\,\text{GeV}$, where most of the data were collected, the correlation with multiplicity is studied as a function of the underlying event transverse sphericity and the number of particles in a cone around the Υ(nS) direction. The ratios are found to be multiplicity independent for jet-like events. The mean $p_{\text{T}}^{\mu\mu}$ values for the Υ(nS) states as a function of particle multiplicity are also measured and found to grow more steeply as their mass increases.

Submitted to the Journal of High Energy Physics

*See Appendix **??** for the list of collaboration members

1 Introduction

A wealth of experimental data on quarkonium production is available [1], but very little of it investigates the relationship to the underlying event (UE). For instance, the fragmentation of soft gluons [2] or feed-down processes [3] (decays of higher-mass states to a lower-mass one), could generate different numbers of particles associated with each of the quarkonium states. Therefore, the global event characteristics (multiplicity, sphericity, etc.) may show variations that depend on the quarkonium state. Recent observations in proton-proton (pp) collisions at the LHC have shown that J/ψ [4] and D [5] meson yields increase with the associated track multiplicity, which has been explained as a consequence of multiparton interactions [6]. The same effect was seen in pp and proton-lead (pPb) collisions [7] for $\Upsilon(\mathrm{nS})$ mesons, where $\mathrm{n} = (1,2,3)$, with the additional observation that this effect is more pronounced for the ground state than for the excited states.

A host of results obtained in pp collisions at the LHC [8–13] may be interpreted as a signal of collective effects in the high particle density environment created at TeV energies [14, 15]. However, it is still not clear whether the small-size system created in pp collisions could exhibit fluid-like properties due to early thermalisation, as observed in PbPb collisions [16, 17]. Some of the collective effects detected so far could possibly be reproduced by fragmentation of saturated gluon states [18] or by the Lund string model [19]. These observations suggest that different phenomena need to be considered for a full understanding of the quarkonium and heavy-flavour production mechanisms. An analysis of the dependence of quarkonium yields as a function of the number of charged particles produced in the event in pp collisions may help to resolve some of these questions [20, 21], in particular in interpreting the observed production rates in heavy ion collisions [22].

In this paper, measurements are presented of the cross section ratios, multiplied by the branching fractions to a muon pair [23], of the bottomonium excited states $\Upsilon(2\mathrm{S})$ and $\Upsilon(3\mathrm{S})$ to the ground state $\Upsilon(1\mathrm{S})$ (indicated by $\Upsilon(2\mathrm{S})/\Upsilon(1\mathrm{S})$ and $\Upsilon(3\mathrm{S})/\Upsilon(1\mathrm{S})$, respectively) as a function of the number of charged particles per event in pp collisions at a centre-of-mass energy of $\sqrt{s} = 7\,\mathrm{TeV}$.

The data were collected in 2011 by the CMS experiment at the LHC. The $\Upsilon(\mathrm{nS})$ states are detected via their dimuon decay in the $\Upsilon(\mathrm{nS})$ rapidity range $|y^{\mu\mu}| < 1.2$. The charged particle multiplicity, N_{track}, is calculated starting from the number of reconstructed tracks with transverse momentum $p_{\mathrm{T}}^{\mathrm{track}} > 0.4\,\mathrm{GeV}$ and pseudorapidity $|\eta^{\mathrm{track}}| < 2.4$, and correcting for the track reconstruction efficiency. Together with the $\Upsilon(\mathrm{nS})$ cross section ratios, the evolution of the average transverse momentum of the Υ states, $\langle p_{\mathrm{T}}^{\mu\mu} \rangle$, is studied with respect to N_{track}. For $p_{\mathrm{T}}^{\mu\mu} > 7\,\mathrm{GeV}$, additional observables are considered to characterise the dependence of the production cross section ratios on N_{track}, including the number of particles produced in various angular regions with respect to the $\Upsilon(\mathrm{nS})$ momentum direction, the number of particles in a restricted cone around this direction, and the transverse sphericity of charged particles in the event.

2 The CMS detector

The central feature of the CMS apparatus is a superconducting solenoid of 6 m internal diameter, providing a magnetic field of 3.8 T. Within the solenoid volume are a silicon pixel and strip tracker, a lead tungstate crystal electromagnetic calorimeter, and a brass and scintillator hadron calorimeter, each composed of a barrel and two endcaps sections. Forward calorimeters extend the η coverage provided by the barrel and endcap detectors. Muons are detected in

gas-ionisation chambers embedded in the steel flux-return yoke outside the solenoid.

The silicon tracker measures charged particles within the range $|\eta^{\text{track}}| < 2.5$. During the LHC running period when the data used in this paper were recorded, the silicon tracker consisted of 1440 silicon pixel and 15 148 silicon strip detector modules. For nonisolated particles of $1 < p_{\text{T}}^{\text{track}} < 10\,\text{GeV}$ and $|\eta^{\text{track}}| < 1.4$, the track resolutions are typically 1.5% in $p_{\text{T}}^{\text{track}}$ and 25–90 (45–150) μm in the transverse (longitudinal) impact parameter [24].

Muons are measured in the range $|\eta^{\mu}| < 2.4$, with detection planes made using three technologies: drift tubes, cathode strip chambers, and resistive plate chambers. Matching muons to tracks measured in the silicon tracker results in a transverse momentum resolution between 1% and 2.8%, for p_{T}^{μ} up to 100 GeV [25].

Events of interest are selected using a two-tiered trigger system [26]. The first level, composed of custom hardware processors, uses information from the calorimeters and muon detectors to select events at a rate of around 100 kHz within a time interval of less than 4 μs. The second level, known as the high-level trigger, consists of a farm of processors running a version of the full event reconstruction software optimised for fast processing, and reduces the event rate to around 1 kHz before data storage.

A more detailed description of the CMS detector, together with a definition of the coordinate system used and the relevant kinematic variables, can be found in Ref. [27].

3 Data analysis

3.1 Event selection

The trigger used to select events for this analysis requires an opposite-sign muon pair with an invariant mass $8.5 < \text{m}_{\mu\mu} < 11.5\,\text{GeV}$, and $|y^{\mu\mu}| < 1.25$, with no explicit p_{T} requirement on the muons. Additionally, the dimuon vertex fit χ^2 probability has to be greater than 0.5% and the distance of closest approach between the two muons less than 5 mm . Events where the two muons bend toward each other in the magnetic field, such that their trajectory can cross within the muon detectors, are rejected to limit the trigger rate, while retaining the highest quality muon pairs. During the 2011 data taking, the increase in the LHC instantaneous luminosity necessitated the increase of the minimum $p_{\text{T}}^{\mu\mu}$ requirement to maintain a constant rate for $\Upsilon(\text{nS})$ events. The collected data correspond to an integrated luminosity of $0.3\,\text{fb}^{-1}$, $1.9\,\text{fb}^{-1}$, and $4.8\,\text{fb}^{-1}$ for minimum $p_{\text{T}}^{\mu\mu}$ requirements of 0, 5, and 7 GeV, respectively. For the inclusive $p_{\text{T}}^{\mu\mu} > 0$ sample, the data are weighted according to the relative integrated luminosity of the period in which they were taken.

In the offline analysis, two reconstructed opposite-sign muon tracks [28] are required to match the triggered muons. Each muon candidate must pass a pseudorapidity-dependent p_{T} requirement with $p_{\text{T}}^{\mu} > 2\,\text{GeV}$ for $1.6 < |\eta^{\mu}| < 2.4$, $p_{\text{T}}^{\mu} > 3.5\,\text{GeV}$ for $|\eta^{\mu}| < 1.2$, and a linear interpolation of the p_{T}^{μ} threshold for $1.2 < |\eta^{\mu}| < 1.6$. Given the $|y^{\mu\mu}|$ trigger constraints, the analysis is restricted to the kinematic region $|y^{\mu\mu}| < 1.2$. In addition, the muon tracks are each required to have at least 11 tracker hits, including at least two hits in the pixel detector. The track fit must have a χ^2 per degree of freedom (ndf) below 1.8 and the tracks must intersect the beam line within a cylinder of radius 3 cm and length ± 30 cm around the detector centre. Finally, the χ^2 probability of the vertex fit must exceed 1%. These selection criteria result in 3 million candidates within the invariant mass range $8.6 < \text{m}_{\mu\mu} < 11.3\,\text{GeV}$ used to extract the signal.

3.2 Track multiplicity evaluation

In 2011, the average number of reconstructed pp collision vertices per bunch crossing (pileup) was seven. The reconstructed pp collision vertex that is closest to the dimuon vertex is considered as the production vertex (PV), and events in which another vertex is located closer than 0.2 cm along the beam line are discarded. This removes 8% of the events. The PV must be located within 10 cm of the centre of the detector along the beamline, where the track reconstruction efficiency is constant.

The contribution of every track to the PV is given as a weight [24]. A track is considered associated if this weight is above 0.5, and the multiplicity is measured by considering the associated tracks that satisfy the high-purity criteria of Ref. [24]. These criteria use the number of silicon tracker layers with hits, the χ^2/ndf of the track fit, and the impact parameter with respect to the beamline to reduce the number of spurious tracks. In addition, the following criteria are designed to check the quality of the tracks and ensure that they emanate from the PV. The transverse and longitudinal impact parameters of each track with respect to the PV must be less than three times the calculated uncertainty in the impact parameter. The tracks must also have a calculated relative p_T uncertainty less than 10%, $|\eta^\mu| < 2.4$, and $p_\mathrm{T}^\mu > 0.4\,\mathrm{GeV}$. The muon tracks are used in the vertex reconstruction, but are not counted in N_track.

Detector effects in track reconstruction are studied with Monte Carlo (MC) samples generated with PYTHIA 8.205 [29] and a UE tune CUETP8M1 [30], using a full simulation of the CMS detector response based on GEANT4 [31]. The MC samples are reconstructed with the same software framework used for the data, including an emulation of the trigger. The track reconstruction efficiency for tracks originating from the PV and within the chosen kinematic region increases from 60% at $p_\mathrm{T}^\mathrm{track} = 0.4\,\mathrm{GeV}$ to greater than 90% for $p_\mathrm{T}^\mathrm{track} > 1\,\mathrm{GeV}$, with an average value of 75%. The rate of misreconstructed tracks (tracks coming from the reconstruction algorithms not matched with a simulated track) is 1–2%. Following the method of Ref. [32], two-dimensional maps in $|\eta^\mathrm{track}|$ and $p_\mathrm{T}^\mathrm{track}$ of the tracker efficiency and misreconstruction rate, are used to produce a factor for each track, given by the complement to 1 of the misreconstruction rate, divided by the efficiency. The N_track value is given by the sum of the associated tracks weighted by this factor. To evaluate the systematic uncertainties in the track multiplicity, correction maps are produced using different types of processes (such as Drell–Yan and multijet events) and another PYTHIA UE tune (4C [33]). The effect on the final N_track is of the order of 1%. This is combined in quadrature with the uncertainty in the tracking efficiency, which is 3.9% for a single track [24]. In the selected data sample, the mean track p_T is around 1.4 GeV and the mean corrected multiplicity $\langle N_\mathrm{track} \rangle = 37.7 \pm 0.1\,(\mathrm{stat}) \pm 1.4\,(\mathrm{syst})$. This multiplicity is about twice the value of 17.8 found in an analysis of minimum bias (MB) events [8], which do not have any selection bias. The average corrected multiplicity is shown for 20 N_track ranges in Table 1. The same binning is used for the $\Upsilon(\mathrm{nS})$ ratios for $p_\mathrm{T}^{\mu\mu} > 7\,\mathrm{GeV}$ as a function of N_track. Different N_track binning has been used for the other results, to take into account the available event statistics with alternative selections.

While the described N_track variable is used for all the results in this paper, to facilitate comparisons with theoretical models, the corresponding true track multiplicity ($N_\mathrm{track}^\mathrm{true}$) was also evaluated, where simulated stable charged particles ($c\tau > 10\,\mathrm{mm}$) are counted. A large Drell–Yan PYTHIA sample was used, which was produced with the same pileup conditions as data. Given the difference in the N_track distribution between data and simulation, the simulation events have been reweighed to reproduce the N_track distribution in data. Then, for every range of N_track, the $N_\mathrm{track}^\mathrm{true}$ distribution is produced both for $p_\mathrm{T}^\mathrm{track} > 0.4\,\mathrm{GeV}$ and $> 0\,\mathrm{GeV}$. These distributions are fitted with two half-Gaussians, which are folded normal distributions having the

same mean and different standard deviations on the left and right sides. The most probable values from the fits are listed in the third and fourth columns of Table 1 for $p_{\mathrm{T}}^{\mathrm{track}} > 0.4\,\mathrm{GeV}$ and 0 GeV, respectively. For $p_{\mathrm{T}}^{\mathrm{track}} > 0.4\,\mathrm{GeV}$ the values are similar to those for $\langle N_{\mathrm{track}} \rangle$, except at high multiplicity. This is due to the probability of merging two nearby vertices during reconstruction, which moves events from low to high multiplicity. Using the same PYTHIA simulation, where a merged vertex can be easily tagged by comparison with the generator-level information, we find that for the 2011 pileup conditions the percentage of merged vertices is below 1% for $N_{\mathrm{track}} < 30$, and reaches 13% in the highest-multiplicity bin. Table 1 also reports the percentage of background MB events in data for each multiplicity bin.

Table 1: Efficiency-corrected multiplicity bins used in the Υ(nS) ratio analysis and the corresponding mean number of charged particle tracks with $p_{\mathrm{T}}^{\mathrm{track}} > 0.4\,\mathrm{GeV}$ in the data sample. The most probable values of the two half-Gaussian fit to the corresponding $N_{\mathrm{track}}^{\mathrm{true}}$ in simulation, for $p_{\mathrm{T}}^{\mathrm{track}} > 0.4\,\mathrm{GeV}$ and $p_{\mathrm{T}}^{\mathrm{track}} > 0\,\mathrm{GeV}$, are also indicated. The uncertainties shown are statistical, except for $\langle N_{\mathrm{track}} \rangle$, where the systematic uncertainties are also reported. In the last column, the percentage of minimum bias (MB) events in the different multiplicity bins is also indicated.

N_{track}	$\langle N_{\mathrm{track}} \rangle$	$N_{\mathrm{track}}^{\mathrm{true}}$ $(p_{\mathrm{T}}^{\mathrm{track}} > 0.4\,\mathrm{GeV})$	$N_{\mathrm{track}}^{\mathrm{true}}$ $(p_{\mathrm{T}}^{\mathrm{track}} > 0\,\mathrm{GeV})$	MB (%)
0–6	$4.2 \pm 0.2 \pm 0.1$	4.2 ± 0.3	6.6 ± 0.6	26.94 ± 0.03
6–11	$8.8 \pm 0.4 \pm 0.3$	8.9 ± 0.4	14.9 ± 0.9	16.73 ± 0.03
11–15	$13.1 \pm 0.5 \pm 0.4$	13.4 ± 0.4	22.7 ± 0.9	10.21 ± 0.02
15–19	$17.1 \pm 0.7 \pm 0.6$	17.1 ± 0.4	28.5 ± 0.9	8.39 ± 0.02
19–22	$20.5 \pm 0.8 \pm 0.7$	20.7 ± 0.4	35.4 ± 1.0	5.36 ± 0.02
22–25	$23.5 \pm 0.9 \pm 0.8$	23.5 ± 0.4	40.3 ± 1.0	4.70 ± 0.02
25–28	$26.5 \pm 1.0 \pm 0.9$	26.4 ± 0.4	43.6 ± 1.0	4.12 ± 0.01
28–31	$29.5 \pm 1.2 \pm 1.0$	29.3 ± 0.5	48.5 ± 1.0	3.61 ± 0.01
31–34	$32.5 \pm 1.3 \pm 1.1$	32.2 ± 0.5	53.0 ± 1.0	3.12 ± 0.01
34–37	$35.5 \pm 1.4 \pm 1.2$	35.1 ± 0.5	57.6 ± 1.0	2.72 ± 0.01
37–40	$38.5 \pm 1.5 \pm 1.3$	38.0 ± 0.5	62.1 ± 1.1	2.60 ± 0.01
40–44	$42.0 \pm 1.6 \pm 1.4$	41.3 ± 0.5	67.2 ± 1.1	2.36 ± 0.01
44–48	$45.9 \pm 1.8 \pm 1.5$	45.1 ± 0.6	72.8 ± 1.2	2.21 ± 0.01
48–53	$50.4 \pm 2.0 \pm 1.7$	49.4 ± 0.6	79.1 ± 1.2	2.01 ± 0.01
53–59	$55.8 \pm 2.2 \pm 1.9$	54.4 ± 0.6	86.6 ± 1.2	1.75 ± 0.01
59–67	$62.7 \pm 2.5 \pm 2.1$	60.8 ± 0.6	95.8 ± 1.3	1.41 ± 0.01
67–80	$72.6 \pm 2.9 \pm 2.4$	69.6 ± 0.6	109.2 ± 1.3	1.12 ± 0.01
80–95	$86.0 \pm 3.4 \pm 2.9$	81.9 ± 0.6	126.4 ± 1.4	0.459 ± 0.005
95–110	$100.1 \pm 4.0 \pm 3.3$	95.8 ± 0.9	145.0 ± 1.6	0.121 ± 0.002
110–140	$118.7 \pm 4.9 \pm 3.9$	109.4 ± 1.2	164.5 ± 2.0	0.0038 ± 0.0001

3.3 Signal extraction

In each multiplicity bin listed in Table 1, an extended binned maximum likelihood fit is performed on the dimuon invariant mass distribution, using the ROOFIT toolkit [34]. Each signal peak is described by functions with a Gaussian core and an exponential tail on the low side. The Gaussian core takes into account the reconstructed dimuon mass resolution, which is much larger than the natural widths of the Υ(nS) states. The exponential tail describes the effect from final-state radiation. This function, usually referred to as *GaussExp* [35], is continuous in its value and first derivative. It has two parameters for the mean and width of the Gaussian function and one parameter for the decay constant of the exponential tail. Each peak is fitted with two *GaussExp* functions, which differ only in the widths of the Gaussians, to describe the p_{T} and rapidity dependence of the resolution. The means of the Gaussian functions are constrained to the world-average Υ(nS) masses [23], multiplied by a common free factor to take

into account the slightly shifted experimental dimuon mass scale [25]. The widths of the two Gaussian functions are constrained to scale between the three signal peaks, following the ratios of their world-average masses. The tail parameter of the exponential is left free in the fit, but is common to the three $\Upsilon(nS)$ signal shapes. There are eight resulting free parameters in the fit: the mass scale factor, the two widths of the $\Upsilon(1S)$ Gaussian function, their respective fraction in describing the $\Upsilon(1S)$ peak, the tail parameter of the exponential, the number of $\Upsilon(1S)$ events, and the ratios $\Upsilon(2S)/\Upsilon(1S)$ and $\Upsilon(3S)/\Upsilon(1S)$. The validity of the fit choices, in particular of the fixed mass resolution scaling between the three states, has been confirmed by relaxing these constraints and comparing the results in larger N_{track} bins, to decrease the sensitivity to statistical fluctuations. To describe the background, an *Error Function* combined with an exponential is chosen.

Examples of the invariant mass distributions and the results of the fit are shown in Fig. 1 for $N_{\text{track}} = 0$–6 (left) and 110–140 (right). The lower panel displays the normalised residual (pull) distribution. This is given by the difference between the observed number of events in the data and the integral of the fitted signal and background function in that bin, divided by the Poisson statistical uncertainty in the data. The lineshape description represents the data well and shows no systematic structure. Signal extraction was found to be the main source of systematic uncertainties in the measurement of the ratios. In order to evaluate it, eight alternative fit functions have been considered, combining the described ones and alternative modelling of the signal (Crystal Ball functions [36]) and the background (Chebyshev polynomials of different orders, exponential function). The maximum variation with respect to the chosen fit is taken as the systematic uncertainty, and is found to be up to 5.5% in the highest N_{track} bins.

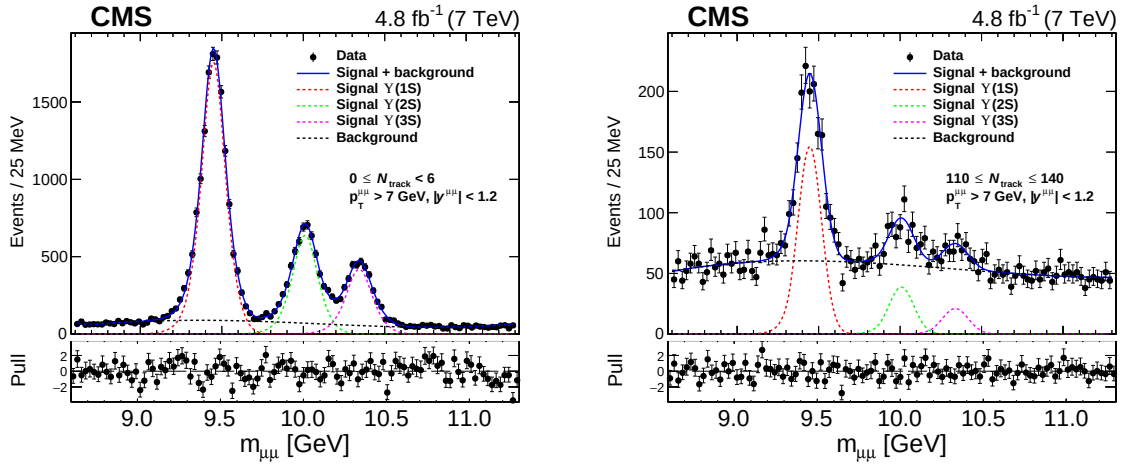

Figure 1: The $\mu^+\,\mu^-$ invariant mass distributions for dimuon candidates with $p_{\text{T}}^{\mu\mu} > 7\,\text{GeV}$ and $|y^{\mu\mu}| < 1.2$, in two intervals of charged particle multiplicity, 0–6 (left) and 110–140 (right). The result of the fit is shown by the solid lines, with the various dotted lines giving the different components. The lower panel displays the pull distribution.

3.4 Acceptances, efficiencies and vertex merging corrections

Evaluation of the efficiencies begins with the single-muon reconstruction efficiencies obtained with a "tag-and-probe" approach [37], based on J/ψ control samples in data. The dimuon efficiency is then obtained by combining the single-muon efficiencies and a factor that takes into account the trigger inefficiency for close-by muons, obtained from MC simulation, following the procedure detailed in Ref. [38].

The acceptances for the three upsilon states are evaluated using an unpolarised hypothesis in the PYTHIA + EVTGEN 1.4.0p1 [39] and PHOTOS 3.56 [40] packages. This hypothesis was chosen since there is no evidence for large $\Upsilon(\mathrm{nS})$ polarisation at LHC energies [41], nor any dependence of the polarisation on multiplicity [42]. No systematic uncertainties are assigned for this assumption.

While the efficiency can be determined event-by-event, the acceptance correction needs to distinguish between the three upsilon states and the background. As a first step, using all the selected candidates, a $p_{\mathrm{T}}^{\mu\mu}$-dependent shape for the efficiency is derived from data. Then, the true $p_{\mathrm{T}}^{\mu\mu}$ distribution from data is extracted using the *sPlot* [43] technique. This method provides an event-by-event weight, based on the value of $\mathrm{m}_{\mu\mu}$, that allows us to reconstruct the $p_{\mathrm{T}}^{\mu\mu}$ distribution, corrected for the background contribution. This experimental $p_{\mathrm{T}}^{\mu\mu}$ distribution for the three $\Upsilon(\mathrm{nS})$ states is rescaled by the $p_{\mathrm{T}}^{\mu\mu}$-dependent efficiency (estimated from data) and acceptance (obtained from simulation). A bin-by-bin correction factor is then calculated as the ratio of the integrals of the rescaled to the original $p_{\mathrm{T}}^{\mu\mu}$ distributions for each bin.

These correction factors show a mild increase with N_{track}. To reduce the statistical fluctuations, a fit is performed with a logistic function to this multiplicity dependence, and the factor used to scale the yields is evaluated at the central N_{track} value in every bin. The difference in the ratio between low- and high-multiplicity bins due to the efficiency and acceptance corrections is of the order of 2%.

The systematic uncertainties due to acceptance and efficiency are calculated by making different choices for their evaluation, and using the new values throughout all the steps of the analysis. For example, alternative procedures are used to estimate the efficiency and acceptance distributions (using simulation instead of collision data for the efficiency calculation, or using different binnings), and the *sPlot* results are compared with those from an invariant mass sideband subtraction method. The only significant effect is found when the mean values of the acceptance and efficiency for all the candidates in a given bin is used instead of the $p_{\mathrm{T}}^{\mu\mu}$-linked correction. This gives a systematic variation in the ratio of the order of 1%.

A final correction to the measured ratios comes from the effect of vertex merging due to pileup. The merging of vertices causes migration of events from lower- to higher-multiplicity bins. It is possible to evaluate the percentage of this migration using simulation. Once a map of the true percentage composition of all the bins is obtained, the ratios can be corrected using an unfolding procedure, starting from the lowest N_{track} bin where no merging affects the ratios. Given that the ratios vary smoothly with N_{track}, the final effect is small, and the largest correction in the highest bin is estimated to be of the order of 1.5%. Systematic uncertainties from different pileup conditions and tunings were found to be negligible.

4 Results and discussion

4.1 The Y(nS) ratios vs. multiplicity

The measured $\Upsilon(2\mathrm{S})/\Upsilon(1\mathrm{S})$ and $\Upsilon(3\mathrm{S})/\Upsilon(1\mathrm{S})$ values are shown in Fig. 2, as a function of N_{track}, for both the (left) $p_{\mathrm{T}}^{\mu\mu} > 7\,\mathrm{GeV}$ ($4.8\,\mathrm{fb}^{-1}$) and (right) $p_{\mathrm{T}}^{\mu\mu} > 0\,\mathrm{GeV}$ (0.3–$4.8\,\mathrm{fb}^{-1}$) samples. In Fig. 2 (right), the CMS results of Ref. [7] for a smaller pp sample at $\sqrt{s} = 2.76\,\mathrm{TeV}$ and in pPb collisions at 5.02 TeV are overlaid on the current results for comparison. In those samples, no p_{T} cut was imposed on the $\Upsilon(\mathrm{nS})$, hence the smaller sample from this analysis starting at $p_{\mathrm{T}} = 0$ is included. A small 2% correction is applied to the present results to account for the different rapidity ranges in the two measurements, based on the measured rapidity dependence of the

Υ(nS) production cross sections [44].

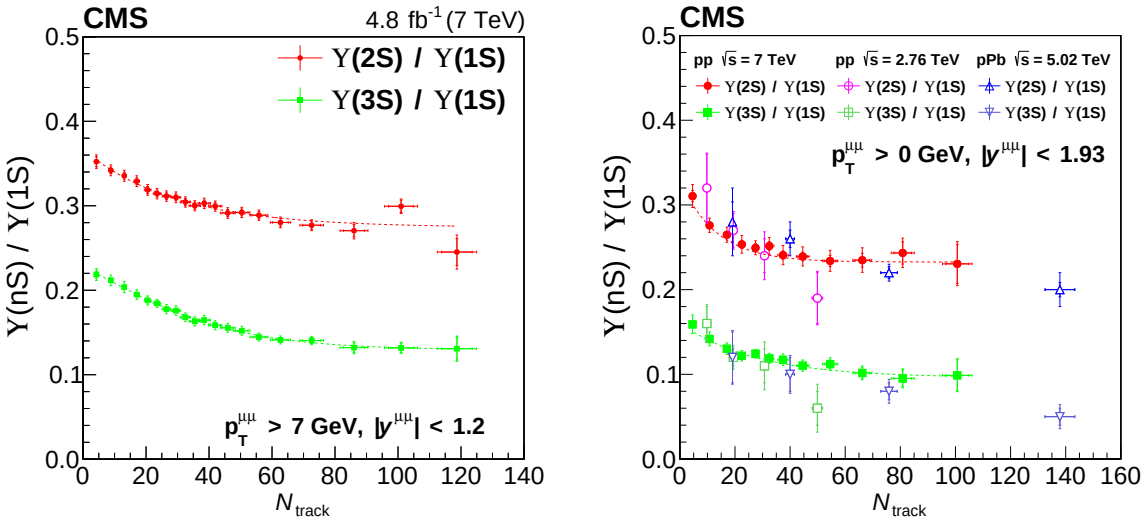

Figure 2: The ratios $\Upsilon(2S)/\Upsilon(1S)$ and $\Upsilon(3S)/\Upsilon(1S)$ with $p_T^{\mu\mu} > 7\,\text{GeV}$ (left) and $p_T^{\mu\mu} > 0\,\text{GeV}$ (right) as a function of N_{track}. The lines are fits to the data with an exponential function. The outer vertical bars represent the combined statistical and systematic uncertainties in the ratios, while the horizontal bars give the uncertainty in $\langle N_{\text{track}} \rangle$ in each bin. Inner tick marks show only the statistical uncertainty, both in the ratio and in $\langle N_{\text{track}} \rangle$. The results of Ref. [7] are shown in the right plot for comparison, and a small correction is applied to the present results to account for the different rapidity ranges in the measurements, $|y^{\mu\mu}| < 1.20$ here and $|y^{\mu\mu}| < 1.93$ in Ref. [7].

A clear trend is visible in both plots with a decrease in the ratios from low- to high-multiplicity bins. The trend is similar in the two kinematic regions, and reminiscent of the measurements from Ref. [7], in particular of the pPb results. To quantify the decrease, a fit is performed using an exponential function: $e^{(p_0+p_1 x)} + p_2$, with p_0, p_1, and p_2 as free parameters in the fit. To measure the decrease in the ratios from this analysis, the resulting best fit is evaluated at the centre of the lowest and highest N_{track} bins. In the $p_T^{\mu\mu} > 7\,\text{GeV}$ case, this results in a decrease of $(-22 \pm 3)\%$ for $\Upsilon(2S)/\Upsilon(1S)$ and $(-42 \pm 4)\%$ for $\Upsilon(3S)/\Upsilon(1S)$, where the uncertainties combine the statistical (evaluated at the 95% confidence level) and systematic (using the upper and lower shifts in the ordinates of the data) uncertainties.

Previous measurements [44] have shown that the ratios $\Upsilon(2S)/\Upsilon(1S)$ and $\Upsilon(3S)/\Upsilon(1S)$ increase with $p_T^{\mu\mu}$. This effect is also visible in Fig. 2, where the values of each ratio are higher in the left plot with a $p_T^{\mu\mu}$ minimum of 7 GeV than in the right plot with no minimum $p_T^{\mu\mu}$ requirement. Figure 3 left (right) shows the mean $p_T^{\mu\mu}$ values for the three Υ(nS) states with $p_T^{\mu\mu} > 7$ (0) GeV, as a function of N_{track}. This is obtained by taking the p_T spectra of the dimuon candidates using the *sPlot* technique and rescaling them for the efficiency and acceptance corrections as a function of $p_T^{\mu\mu}$, as described in Section 3.4. From these corrected $p_T^{\mu\mu}$ distributions the mean value and the corresponding uncertainty are calculated. We observe a hierarchical structure, where the transverse momentum increases more rapidly with N_{track} as the mass of the corresponding Υ(nS) increases. An increase with particle mass was also observed in pp collisions at the LHC for pions, kaons, and protons [45].

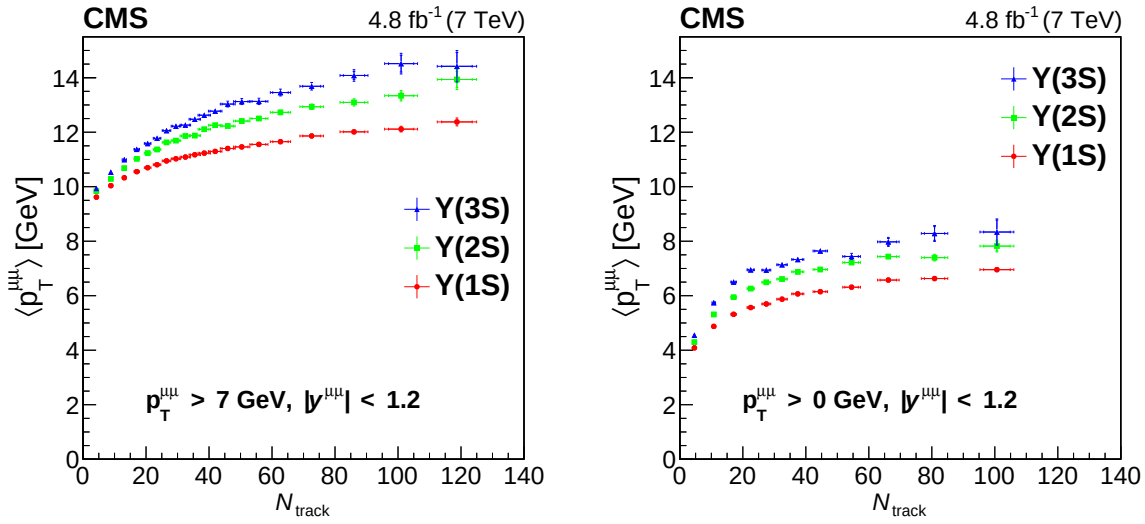

Figure 3: Mean $p_{\mathrm{T}}^{\mu\mu}$ values for the three $\Upsilon(\mathrm{nS})$ states as a function of N_{track} for $p_{\mathrm{T}}^{\mu\mu} > 7\,\mathrm{GeV}$ (left) and $> 0\,\mathrm{GeV}$ (right). The outer vertical bars represent the combined statistical and systematic uncertainties in the ratios, while the horizontal bars give the uncertainty in $\langle N_{\mathrm{track}} \rangle$ in each bin. Inner tick marks show only the statistical uncertainty, both in the ratio and in $\langle N_{\mathrm{track}} \rangle$.

4.2 Transverse momentum dependence

The ratios $\Upsilon(2\mathrm{S})/\Upsilon(1\mathrm{S})$ (left) and $\Upsilon(3\mathrm{S})/\Upsilon(1\mathrm{S})$ (right) are plotted in Fig. 4 as a function of N_{track} for seven $p_{\mathrm{T}}^{\mu\mu}$ intervals from 0 to 50 GeV.

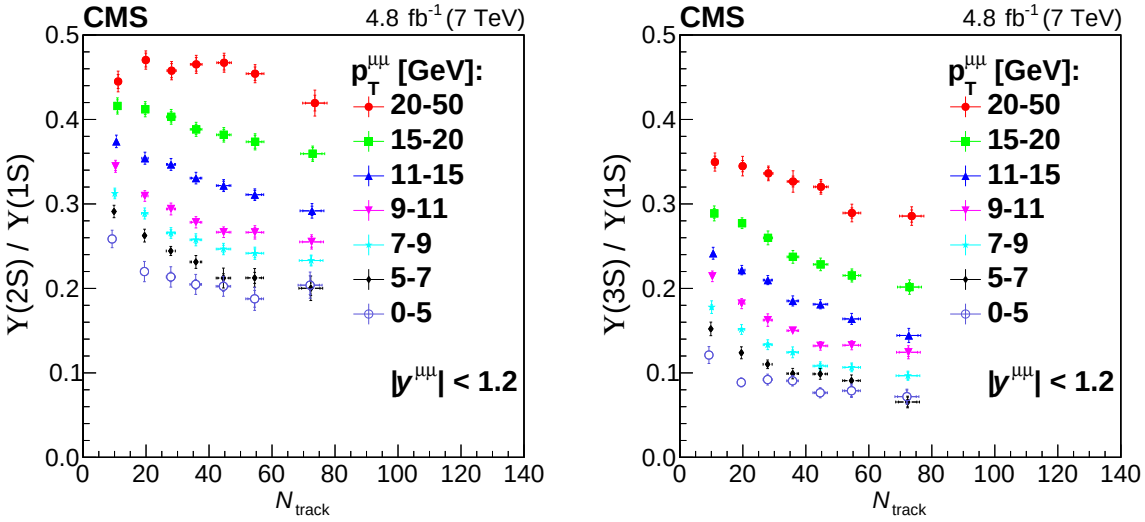

Figure 4: The ratios $\Upsilon(2\mathrm{S})/\Upsilon(1\mathrm{S})$ (left) and $\Upsilon(3\mathrm{S})/\Upsilon(1\mathrm{S})$ (right) as a function of N_{track}, for different $p_{\mathrm{T}}^{\mu\mu}$ intervals. The interval 0–5 GeV corresponds to an integrated luminosity of $0.3\,\mathrm{fb}^{-1}$, the interval 5–7 GeV to $1.9\,\mathrm{fb}^{-1}$, and the rest to the full integrated luminosity of $4.8\,\mathrm{fb}^{-1}$. The outer vertical bars represent the combined statistical and systematic uncertainties in the ratios, while the horizontal bars give the uncertainty in $\langle N_{\mathrm{track}} \rangle$ in each bin. Inner tick marks show only the statistical uncertainty, both in the ratio and in $\langle N_{\mathrm{track}} \rangle$.

In all the $p_{\mathrm{T}}^{\mu\mu}$ ranges, there is a decrease in the ratios with increasing multiplicity, with the largest rate of decrease in the $p_{\mathrm{T}}^{\mu\mu} = 5$–7 GeV bin. At higher $p_{\mathrm{T}}^{\mu\mu}$ values, the decrease in the ratios is smaller. This is particularly evident for the $p_{\mathrm{T}}^{\mu\mu} = 20$–50 GeV bin, especially for $\Upsilon(2\mathrm{S})/\Upsilon(1\mathrm{S})$ where the ratio is compatible with being constant. In the 0–5 GeV bin, all the

decrease occurs at low multiplicity, with the ratios consistent with being flat beyond the first N_{track} bin, especially for the ratio $\Upsilon(2S)/\Upsilon(1S)$.

4.3 Local multiplicity dependence

To better investigate the connection between $\Upsilon(nS)$ production and the UE properties, a new type of multiplicity, $N_{\text{track}}^{\Delta\phi}$, is defined, based on the difference between the azimuthal angle of each track and the $\Upsilon(nS)$ meson, $\Delta\phi$. This relative angular separation is divided into three ranges (as is done in Ref. [46]): a *forward* one comprised of $|\Delta\phi| < \pi/3$ radians, a *transverse* one with $\pi/3 \leq |\Delta\phi| < 2\pi/3$ radians, and a *backward* one of $2\pi/3 \leq |\Delta\phi| \leq \pi$ radians, as shown in Fig. 5 (left).

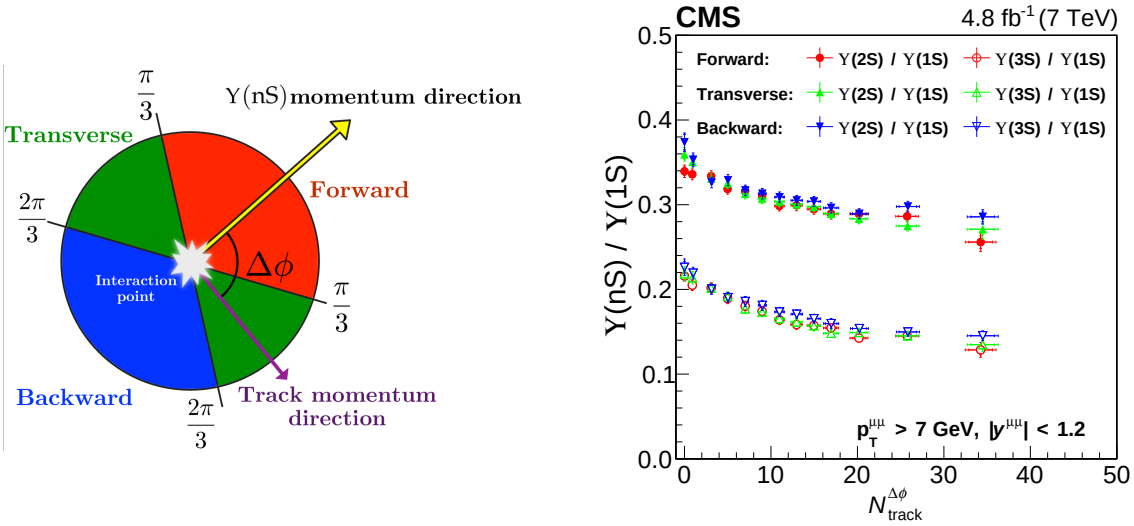

Figure 5: Left: A schematic view in the azimuthal plane of the three $\Delta\phi$ regions with respect to the $\Upsilon(nS)$ momentum direction. Right: The ratios $\Upsilon(2S)/\Upsilon(1S)$ and $\Upsilon(3S)/\Upsilon(1S)$, as a function of $N_{\text{track}}^{\Delta\phi}$ for the three $\Delta\phi$ regions shown in the left plot. The outer vertical bars represent the combined statistical and systematic uncertainties in the ratios, while the horizontal bars give the uncertainty in $\langle N_{\text{track}}^{\Delta\phi} \rangle$ for each bin. Inner tick marks show only the statistical uncertainty, both in the ratio and in $\langle N_{\text{track}}^{\Delta\phi} \rangle$.

On average, there are about three more tracks in the *forward* (14.55 ± 0.05, including the two muons) and *backward* (14.83 ± 0.05) regions than in the *transverse* interval (11.90 ± 0.05), where the uncertainties are statistical only. Similar values are obtained when considering the $\Upsilon(1S)$, $\Upsilon(2S)$, and $\Upsilon(3S)$ mesons separately.

The $\Upsilon(nS)$ ratios are presented as a function of $N_{\text{track}}^{\Delta\phi}$ in the three azimuthal intervals in Fig. 5 (right), where the decrease in the ratios is again visible, with similar trends in the three angular regions. The main differences are present at low $N_{\text{track}}^{\Delta\phi}$, where the ratios are slightly higher when considering the backward azimuthal region. In particular, the fact that the decrease is present in the transverse region suggests its connection with the UE itself, rather than a dependence on the particle activity along the $\Upsilon(nS)$ direction, which would produce additional particles only in the forward region. The same consideration applies to unaccounted effects coming from feed-down, i.e. from $\Upsilon(nS)$ states not produced in the hard scatter, as discussed in the following section.

4.4 Dependence on the Y(nS) isolation

The isolation of the $\Upsilon(\mathrm{nS})$ is defined by the number of tracks found in a small angular region around its direction. The study is aimed at verifying whether charged tracks produced along the Υ momentum direction, such as the "comovers" of Ref. [47], could explain the observed reduction in the cross section ratio. The number of particles ($N_{\mathrm{track}}^{\Delta R}$) in a cone around the Υ momentum direction ($\Delta\mathrm{R} = \sqrt{(\Delta\eta)^2 + (\Delta\phi)^2} < 0.5$) is counted, where $\Delta\eta$ is the difference in pseudorapidity between the $\Upsilon(\mathrm{nS})$ and the other particles. The data sample is split into four categories: $N_{\mathrm{track}}^{\Delta R} = 0, 1, 2$, and > 2. In the last case, for the lower multiplicity range 0–15, a strong decrease in both ratios was initially observed. The source was identified as an enhancement of the $\Upsilon(1\mathrm{S})$ signal coming from the feed-down process $\Upsilon(2\mathrm{S}) \to \Upsilon(1\mathrm{S})\pi^+\pi^-$. This was verified by reconstructing the $\Upsilon(2\mathrm{S})$ state using the selection and procedure of Ref. [48]. While the raw number of reconstructed $\Upsilon(2\mathrm{S})$ events from the fit to the $\Upsilon(1\mathrm{S})\pi^+\pi^-$ mass spectrum is below 1% in all the N_{track} bins, this component increases significantly, up to 25%, when we require tracks in the $\Delta\mathrm{R} < 0.5$ cone. On the other hand, the contributions from $\Upsilon(3\mathrm{S}) \to \Upsilon(1\mathrm{S})\pi^+\pi^-$ and $\Upsilon(3\mathrm{S}) \to \Upsilon(2\mathrm{S})\pi^+\pi^-$ decays remain negligible. A correction is applied to take into account both the number of reconstructed feed-down events and the probability that an event is selected in that multiplicity bin due to the presence of the feed-down $\pi^+\pi^-$ pair. A sizeable (of the order of 30%) correction is needed only for the N_{track} = 0–15 bin, when requiring more than two particles in the cone. The ratios $\Upsilon(2\mathrm{S})/\Upsilon(1\mathrm{S})$ and $\Upsilon(3\mathrm{S})/\Upsilon(1\mathrm{S})$ vs. track multiplicity in the four different categories, after this correction, are shown in Fig. 6 (left). The dependence on the charged particle multiplicity is similar in all the categories and also shows a flattening in the $N_{\mathrm{track}}^{\Delta R} > 2$ category, which is opposite to what would be expected in the comover picture.

4.5 Transverse sphericity dependence

The transverse sphericity is a momentum-space variable, useful in distinguishing the dominant physics process in the interaction. It is defined as:

$$S_{\mathrm{T}} \equiv \frac{2\lambda_2}{\lambda_1 + \lambda_2},$$

where $\lambda_1 > \lambda_2$ are the eigenvalues of the matrix constructed from the transverse momenta components of the charged particles (labelled with the index i), linearised by the additional term $1/p_{\mathrm{T}i}$ (following Ref. [49]):

$$S_{xy}^{T} = \frac{1}{\sum_i p_{\mathrm{T}i}} \sum_i \frac{1}{p_{\mathrm{T}i}} \begin{pmatrix} p_{xi}^2 & p_{xi}p_{yi} \\ p_{xi}p_{yi} & p_{yi}^2 \end{pmatrix}.$$

By construction, an isotropic event has sphericity close to 1 ("high" sphericity), while "jet-like" events have S_{T} close to zero. For very low multiplicity, S_{T} tends to take low values, so its definition is inherently multiplicity dependent. The cross section ratio between the $\Upsilon(\mathrm{nS})$ states is evaluated as a function of multiplicity in four transverse sphericity intervals, 0–0.55, 0.55–0.70, 0.70–0.85, and 0.85–1.00. The resulting trends are shown in Fig. 6 (right). In the low-sphericity region, the ratios remain nearly independent of multiplicity, while the three bins with $S_{\mathrm{T}} > 0.55$ show a similar decrease as a function of multiplicity. This observation suggests that the decrease in the ratios is an UE effect. When the high multiplicity is due to the presence of jets or other localised objects and S_{T} is small, the decrease is absent. It can also help to explain why the multiplicity dependence is almost flat at higher $p_{\mathrm{T}}^{\mu\mu}$, as shown in Fig. 4. This is because low-sphericity events have a higher $p_{\mathrm{T}}^{\mu\mu}$ on average.

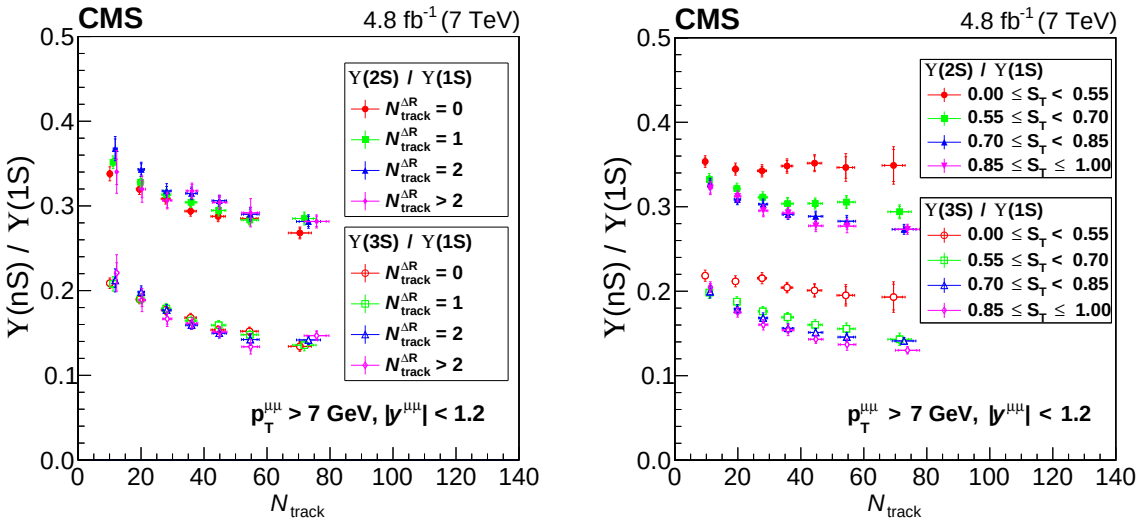

Figure 6: The ratios $\Upsilon(2S)/\Upsilon(1S)$ and $\Upsilon(3S)/\Upsilon(1S)$ are shown as a function of the track multiplicity N_{track}: in four categories based on the number of charged particles produced in a $\Delta R < 0.5$ cone around the Υ direction (left), and in different intervals of charged particle transverse sphericity, S_T (right). The outer vertical bars represent the combined statistical and systematic uncertainties in the ratios, while the horizontal bars give the uncertainty in $\langle N_{\text{track}} \rangle$ in each bin. Inner tick marks show only the statistical uncertainty, both in the ratio and in $\langle N_{\text{track}} \rangle$.

4.6 Discussion

The impact of additional UE particles on the trend of the Υ cross section ratios to decrease with multiplicity in pp and pPb collisions was pointed out in Ref. [7]. In particular, it was noted that the events containing the ground state had about two more tracks on average than the ones containing the excited states. It was concluded that the feed-down contributions cannot solely account for this feature. This is also seen in the present analysis, where the $\Upsilon(1S)$ meson is accompanied by about one more track on average ($\langle N_{\text{track}} \rangle = 33.9 \pm 0.1$) than the $\Upsilon(2S)$ ($\langle N_{\text{track}} \rangle = 33.0 \pm 0.1$), and about two more than the $\Upsilon(3S)$ ($\langle N_{\text{track}} \rangle = 32.0 \pm 0.1$). However, as seen in Fig. 6 (left), no significant change is seen when keeping only events with no tracks within a cone along the $\Upsilon(nS)$ direction.

One could argue that, given the same energy of a parton collision, the lower mass of the upsilon ground state compared to the excited states would leave more energy available for the production of accompanying particles. On the other hand, it is also true that, if we expect a suppression of the excited states at high multiplicity, it would also appear as a shift in the mean number of particles for that state (because events at higher multiplicities would be missing). Furthermore, if we consider only the events with $0 < S_T < 0.55$, where none or little dependence on multiplicity is present, the mean number of charged particles per event is exactly the same for the three Υ states ($\langle N_{\text{track}} \rangle = 22.4 \pm 0.1$). This suggests that the different number of associated particles is not directly linked to the difference in mass between the three states.

5 Summary

The measurement of ratios of the $\Upsilon(nS) \to \mu^+\mu^-$ yields in proton-proton collisions at $\sqrt{s} = 7\,\text{TeV}$, corresponding to an integrated luminosity of $4.8\,\text{fb}^{-1}$, collected with the CMS detector at the LHC, are reported as a function of the number of charged particles produced with pseu-

dorapidity $|\eta^{\text{track}}| < 2.4$ and transverse momentum $p_{\text{T}}^{\text{track}} > 0.4\,\text{GeV}$. A significant reduction of the $\Upsilon(2S)/\Upsilon(1S)$ and $\Upsilon(3S)/\Upsilon(1S)$ production ratios is observed with increasing multiplicity. This result confirms the observation made in proton-proton and proton-lead collisions at lower centre-of-mass energy [7], with increased precision. The effect is present in different ranges of $p_{\text{T}}^{\mu\mu}$, but decreases with increasing $p_{\text{T}}^{\mu\mu}$. For $p_{\text{T}}^{\mu\mu} > 7\,\text{GeV}$, different observables are studied in order to obtain a better description of the phenomenon in connection with the underlying event. No variation in the decrease of the ratios is found by changing the azimuthal angle separation of the charged particles with respect to the Υ momentum direction. The same applies when varying the number of tracks in a restricted cone around the Υ momentum direction. However, the ratios are observed to be multiplicity independent for jet-like events. The presented results give for the first time a comprehensive review of the connection between $\Upsilon(nS)$ production and the underlying event, stressing the need for an improved theoretical description of quarkonium production in proton-proton collisions.

Acknowledgments

We congratulate our colleagues in the CERN accelerator departments for the excellent performance of the LHC and thank the technical and administrative staffs at CERN and at other CMS institutes for their contributions to the success of the CMS effort. In addition, we gratefully acknowledge the computing centres and personnel of the Worldwide LHC Computing Grid for delivering so effectively the computing infrastructure essential to our analyses. Finally, we acknowledge the enduring support for the construction and operation of the LHC and the CMS detector provided by the following funding agencies: BMBWF and FWF (Austria); FNRS and FWO (Belgium); CNPq, CAPES, FAPERJ, FAPERGS, and FAPESP (Brazil); MES (Bulgaria); CERN; CAS, MoST, and NSFC (China); COLCIENCIAS (Colombia); MSES and CSF (Croatia); RIF (Cyprus); SENESCYT (Ecuador); MoER, ERC IUT, PUT and ERDF (Estonia); Academy of Finland, MEC, and HIP (Finland); CEA and CNRS/IN2P3 (France); BMBF, DFG, and HGF (Germany); GSRT (Greece); NKFIA (Hungary); DAE and DST (India); IPM (Iran); SFI (Ireland); INFN (Italy); MSIP and NRF (Republic of Korea); MES (Latvia); LAS (Lithuania); MOE and UM (Malaysia); BUAP, CINVESTAV, CONACYT, LNS, SEP, and UASLP-FAI (Mexico); MOS (Montenegro); MBIE (New Zealand); PAEC (Pakistan); MSHE and NSC (Poland); FCT (Portugal); JINR (Dubna); MON, RosAtom, RAS, RFBR, and NRC KI (Russia); MESTD (Serbia); SEIDI, CPAN, PCTI, and FEDER (Spain); MOSTR (Sri Lanka); Swiss Funding Agencies (Switzerland); MST (Taipei); ThEPCenter, IPST, STAR, and NSTDA (Thailand); TUBITAK and TAEK (Turkey); NASU (Ukraine); STFC (United Kingdom); DOE and NSF (USA).

Individuals have received support from the Marie-Curie programme and the European Research Council and Horizon 2020 Grant, contract Nos. 675440, 752730, and 765710 (European Union); the Leventis Foundation; the A.P. Sloan Foundation; the Alexander von Humboldt Foundation; the Belgian Federal Science Policy Office; the Fonds pour la Formation à la Recherche dans l'Industrie et dans l'Agriculture (FRIA-Belgium); the Agentschap voor Innovatie door Wetenschap en Technologie (IWT-Belgium); the F.R.S.-FNRS and FWO (Belgium) under the "Excellence of Science – EOS" – be.h project n. 30820817; the Beijing Municipal Science & Technology Commission, No. Z191100007219010; the Ministry of Education, Youth and Sports (MEYS) of the Czech Republic; the Deutsche Forschungsgemeinschaft (DFG) under Germany's Excellence Strategy – EXC 2121 "Quantum Universe" – 390833306; the Lendület ("Momentum") Programme and the János Bolyai Research Scholarship of the Hungarian Academy of Sciences, the New National Excellence Program ÚNKP, the NKFIA research grants 123842, 123959, 124845, 124850, 125105, 128713, 128786, and 129058 (Hungary); the Council of Science and Industrial Research, India; the HOMING PLUS programme of the Foundation for

Polish Science, cofinanced from European Union, Regional Development Fund, the Mobility Plus programme of the Ministry of Science and Higher Education, the National Science Center (Poland), contracts Harmonia 2014/14/M/ST2/00428, Opus 2014/13/B/ST2/02543, 2014/15/B/ST2/03998, and 2015/19/B/ST2/02861, Sonata-bis 2012/07/E/ST2/01406; the National Priorities Research Program by Qatar National Research Fund; the Ministry of Science and Higher Education, project no. 02.a03.21.0005 (Russia); the Programa Estatal de Fomento de la Investigación Científica y Técnica de Excelencia María de Maeztu, grant MDM-2015-0509 and the Programa Severo Ochoa del Principado de Asturias; the Thalis and Aristeia programmes cofinanced by EU-ESF and the Greek NSRF; the Rachadapisek Sompot Fund for Postdoctoral Fellowship, Chulalongkorn University and the Chulalongkorn Academic into Its 2nd Century Project Advancement Project (Thailand); the Kavli Foundation; the Nvidia Corporation; the SuperMicro Corporation; the Welch Foundation, contract C-1845; and the Weston Havens Foundation (USA).

References

[1] A. Andronic et al., "Heavy-flavour and quarkonium production in the LHC era: From proton-proton to heavy-ion collisions", *Eur. Phys. J. C* **76** (2016) 107, doi:10.1140/epjc/s10052-015-3819-5, arXiv:1506.03981.

[2] M. Krämer, "Quarkonium production at high-energy colliders", *Prog. Part. Nucl. Phys.* **47** (2001) 141, doi:10.1016/S0146-6410(01)00154-5, arXiv:hep-ph/0106120.

[3] S. Digal, P. Petreczky, and H. Satz, "Quarkonium feed-down and sequential suppression", *Phys. Rev. D* **64** (2001) 094015, doi:10.1103/PhysRevD.64.094015, arXiv:hep-ph/0106017.

[4] ALICE Collaboration, "J/ψ production as a function of charged particle multiplicity in pp collisions at $\sqrt{s} = 7$ TeV", *Phys. Lett. B* **712** (2012) 165, doi:10.1016/j.physletb.2012.04.052, arXiv:1202.2816.

[5] ALICE Collaboration, "D-meson production in pPb collisions at $\sqrt{s_{\rm NN}} = 5.02$ TeV and in pp collisions at $\sqrt{s} = 7$ TeV", *Phys. Rev. C* **94** (2016) 054908, doi:10.1103/PhysRevC.94.054908, arXiv:1605.07569.

[6] D. Thakur, S. De, R. Sahoo, and S. Dansana, "Role of multiparton interactions on J/ψ production in pp collisions at LHC energies", *Phys. Rev. D* **97** (2018) 094002, doi:10.1103/PhysRevD.97.094002, arXiv:1709.06358.

[7] CMS Collaboration, "Event activity dependence of Υ(nS) production in $\sqrt{s_{\rm NN}} = 5.02$ TeV pPb and $\sqrt{s} = 2.76$ TeV pp collisions", *JHEP* **04** (2014) 103, doi:10.1007/JHEP04(2014)103, arXiv:1312.6300.

[8] CMS Collaboration, "Observation of long-range near-side angular correlations in proton-proton collisions at the LHC", *JHEP* **09** (2010) 091, doi:10.1007/JHEP09(2010)091, arXiv:1009.4122.

[9] ATLAS Collaboration, "Observation of long-range elliptic azimuthal anisotropies in $\sqrt{s} = 13$ and 2.76 TeV pp collisions with the ATLAS detector", *Phys. Rev. Lett.* **116** (2016) 172301, doi:10.1103/PhysRevLett.116.172301, arXiv:1509.04776.

[10] CMS Collaboration, "Measurement of long-range near-side two-particle angular correlations in pp collisions at $\sqrt{s} = 13\,\text{TeV}$", *Phys. Rev. Lett.* **116** (2016) 172302, doi:10.1103/PhysRevLett.116.172302, arXiv:1510.03068.

[11] ALICE Collaboration, "Enhanced production of multi-strange hadrons in high-multiplicity proton-proton collisions", *Nature Phys.* **13** (2017) 535, doi:10.1038/nphys4111, arXiv:1606.07424.

[12] CMS Collaboration, "Evidence for collectivity in pp collisions at the LHC", *Phys. Lett. B* **765** (2017) 193, doi:10.1016/j.physletb.2016.12.009, arXiv:1606.06198.

[13] CMS Collaboration, "Multiplicity and rapidity dependence of strange hadron production in pp, pPb, and PbPb collisions at the LHC", *Phys. Lett. B* **768** (2017) 103, doi:10.1016/j.physletb.2017.01.075, arXiv:1605.06699.

[14] R. Campanini and G. Ferri, "Experimental equation of state in proton-proton and proton-antiproton collisions and phase transition to quark gluon plasma", *Phys. Lett. B* **703** (2011) 237, doi:10.1016/j.physletb.2011.08.009, arXiv:1106.2008.

[15] K. Dusling, W. Li, and B. Schenke, "Novel collective phenomena in high-energy proton-proton and proton-nucleus collisions", *Int. J. Mod. Phys. E* **25** (2016) 1630002, doi:10.1142/S0218301316300022, arXiv:1509.07939.

[16] F. G. Gardim, G. Giacalone, M. Luzum, and J.-Y. Ollitrault, "Thermodynamics of hot strong-interaction matter from ultrarelativistic nuclear collisions", *Nature Phys.* **16** (2020) 615, doi:10.1038/s41567-020-0846-4.

[17] J. L. Nagle and W. A. Zajc, "Small system collectivity in relativistic hadronic and nuclear collisions", *Ann. Rev. Nucl. Part. Sci.* **68** (2018) 211, doi:10.1146/annurev-nucl-101916-123209, arXiv:1801.03477.

[18] B. Schenke, S. Schlichting, P. Tribedy, and R. Venugopalan, "Mass ordering of spectra from fragmentation of saturated gluon states in high multiplicity proton-proton collisions", *Phys. Rev. Lett.* **117** (2016) 162301, doi:10.1103/PhysRevLett.117.162301, arXiv:1607.02496.

[19] S. Ferreres-Solé and T. Sjöstrand, "The space-time structure of hadronization in the Lund model", *Eur. Phys. J. C* **78** (2018) 983, doi:10.1140/epjc/s10052-018-6459-8, arXiv:1808.04619.

[20] T. Lang and M. Bleicher, "Possibility for J/ψ suppression in high multiplicity proton-proton collisions at $\sqrt{s_{\text{NN}}} = 7$ TeV", *Phys. Rev. C* **87** (2013) 024907, doi:10.1103/PhysRevC.87.024907, arXiv:1302.0655.

[21] E. G. Ferreiro and C. Pajares, "High multiplicity pp events and J/ψ production at LHC", *Phys. Rev. C* **86** (2012) 034903, doi:10.1103/PhysRevC.86.034903, arXiv:1203.5936.

[22] CMS Collaboration, "Measurement of nuclear modification factors of $\Upsilon(1S)$, $\Upsilon(2S)$, and $\Upsilon(3S)$ mesons in PbPb collisions at $\sqrt{s_{\text{NN}}} = 5.02$ TeV", *Phys. Lett. B* **790** (2019) 270, doi:10.1016/j.physletb.2019.01.006, arXiv:1805.09215.

[23] Particle Data Group, M. Tanabashi et al., "Review of particle physics", *Phys. Rev. D* **98** (2018) 030001, doi:10.1103/PhysRevD.98.030001.

[24] CMS Collaboration, "Description and performance of track and primary-vertex reconstruction with the CMS tracker", *JINST* **9** (2014) P10009, doi:10.1088/1748-0221/9/10/P10009, arXiv:1405.6569.

[25] CMS Collaboration, "Performance of CMS muon reconstruction in pp collision events at $\sqrt{s} = 7$ TeV", *JINST* **7** (2012) P10002, doi:10.1088/1748-0221/7/10/P10002, arXiv:1206.4071.

[26] CMS Collaboration, "The CMS trigger system", *JINST* **12** (2017) P01020, doi:10.1088/1748-0221/12/01/P01020, arXiv:1609.02366.

[27] CMS Collaboration, "The CMS experiment at the CERN LHC", *JINST* **3** (2008) S08004, doi:10.1088/1748-0221/3/08/S08004.

[28] CMS Collaboration, "The performance of the CMS muon detector in proton-proton collisions at $\sqrt{s} = 7$ TeV at the LHC", *JINST* **8** (2013) P11002, doi:10.1088/1748-0221/8/11/P11002, arXiv:1306.6905.

[29] T. Sjöstrand et al., "An introduction to PYTHIA 8.2", *Comput. Phys. Commun.* **191** (2015) 159, doi:10.1016/j.cpc.2015.01.024, arXiv:1410.3012.

[30] CMS Collaboration, "Event generator tunes obtained from underlying event and multiparton scattering measurements", *Eur. Phys. J. C* **76** (2016) 155, doi:10.1140/epjc/s10052-016-3988-x, arXiv:1512.00815.

[31] GEANT4 Collaboration, "GEANT4—a simulation toolkit", *Nucl. Instrum. Meth. A* **506** (2003) 250, doi:10.1016/S0168-9002(03)01368-8.

[32] CMS Collaboration, "Jet and underlying event properties as a function of charged-particle multiplicity in proton-proton collisions at $\sqrt{s} = 7$ TeV", *Eur. Phys. J. C* **73** (2013) 2674, doi:10.1140/epjc/s10052-013-2674-5, arXiv:1310.4554.

[33] R. Corke and T. Sjöstrand, "Interleaved parton showers and tuning prospects", *JHEP* **03** (2011) 032, doi:10.1007/JHEP03(2011)032, arXiv:1011.1759.

[34] W. Verkerke and D. P. Kirkby, "The RooFit toolkit for data modeling", in *13th International Conference for Computing in High-Energy and Nuclear Physics (CHEP03)*. 2003. arXiv:physics/0306116. CHEP-2003-MOLT007.

[35] S. Das, "A simple alternative to the Crystal Ball function", (2016). arXiv:1603.08591.

[36] M. J. Oreglia, "A study of the reactions $\psi' \to \gamma\gamma\psi$". PhD thesis, Stanford University, 1980. SLAC Report SLAC-R-236.

[37] CMS Collaboration, "Measurements of inclusive W and Z cross sections in pp collisions at $\sqrt{s} = 7$ TeV", *JHEP* **01** (2011) 080, doi:10.1007/JHEP01(2011)080, arXiv:1012.2466.

[38] CMS Collaboration, "Measurements of the $\Upsilon(1S)$, $\Upsilon(2S)$, and $\Upsilon(3S)$ differential cross sections in pp collisions at $\sqrt{s} = 7$ TeV", *Phys. Lett. B* **749** (2015) 14, doi:10.1016/j.physletb.2015.07.037, arXiv:1501.07750.

[39] D. J. Lange, "The EVTGEN particle decay simulation package", in *Proceedings, 7th International Conference on B physics at hadron machines (BEAUTY 2000): Maagan, Israel, September 13-18, 2000*, volume 462, p. 152. 2001. doi:10.1016/S0168-9002(01)00089-4.

[40] E. Barberio and Z. Wąs, "PHOTOS – a universal Monte Carlo for QED radiative corrections: Version 2.0", *Comput. Phys. Commun.* **79** (1994) 291, doi:10.1016/0010-4655(94)90074-4.

[41] CMS Collaboration, "Measurement of the $\Upsilon(1S)$, $\Upsilon(2S)$, and $\Upsilon(3S)$ polarizations in pp collisions at $\sqrt{s} = 7$ TeV", *Phys. Rev. Lett.* **110** (2013) 081802, doi:10.1103/PhysRevLett.110.081802, arXiv:1209.2922.

[42] CMS Collaboration, "$\Upsilon(nS)$ polarizations versus particle multiplicity in pp collisions at $\sqrt{s} = 7$ TeV", *Phys. Lett. B* **761** (2016) 31, doi:10.1016/j.physletb.2016.07.065, arXiv:1603.02913.

[43] M. Pivk and F. R. Le Diberder, "sPlot: A statistical tool to unfold data distributions", *Nucl. Instrum. Meth. A* **555** (2005) 356, doi:10.1016/j.nima.2005.08.106, arXiv:physics/0402083.

[44] CMS Collaboration, "Measurement of the $\Upsilon(1S)$, $\Upsilon(2S)$, and $\Upsilon(3S)$ cross sections in pp collisions at $\sqrt{s} = 7$ TeV", *Phys. Lett. B* **727** (2013) 101, doi:10.1016/j.physletb.2013.10.033, arXiv:1303.5900.

[45] CMS Collaboration, "Study of the inclusive production of charged pions, kaons, and protons in pp collisions at $\sqrt{s} = 0.9$, 2.76, and 7 TeV", *Eur. Phys. J. C* **72** (2012) 2164, doi:10.1140/epjc/s10052-012-2164-1, arXiv:1207.4724.

[46] CMS Collaboration, "First measurement of the underlying event activity at the LHC with $\sqrt{s} = 0.9$ TeV", *Eur. Phys. J. C* **70** (2010) 555, doi:10.1140/epjc/s10052-010-1453-9, arXiv:1006.2083.

[47] E. G. Ferreiro, "Charmonium dissociation and recombination at LHC: Revisiting comovers", *Phys. Lett. B* **731** (2014) 57, doi:10.1016/j.physletb.2014.02.011, arXiv:1210.3209.

[48] CMS Collaboration, "Search for a new bottomonium state decaying to $\Upsilon(1S)\pi^+\pi^-$ in pp collisions at $\sqrt{s} = 8$ TeV", *Phys. Lett. B* **727** (2013) 57, doi:10.1016/j.physletb.2013.10.016, arXiv:1309.0250.

[49] ALICE Collaboration, "Transverse sphericity of primary charged particles in minimum bias proton-proton collisions at $\sqrt{s} = 0.9$, 2.76, and 7 TeV", *Eur. Phys. J. C* **72** (2012) 2124, doi:10.1140/epjc/s10052-012-2124-9, arXiv:1205.3963.